J. Fluid Mech. (1981), *vol.* 102, *pp.* 61–74
Printed in Great Britain

Low-Prandtl-number convection in a layer heated from below

By R. M. CLEVER AND F. H. BUSSE

Institute of Geophysics and Planetary Physics and Department of Earth and Space Sciences, University of California, Los Angeles, California 90024, U.S.A.

(Received 5 November 1979 and in revised form 5 March 1980)

Steady solutions in the form of two-dimensional rolls are obtained numerically for convection in a horizontal layer of a low-Prandtl-number fluid heated from below. Prandtl numbers in the range $0{\cdot}001 \leqslant P \leqslant 0{\cdot}71$ are investigated for Rayleigh numbers between the critical value, $R = 1708$, and $R = 20{,}000$ in the case of rigid boundaries. The calculations reveal that the convective heat transport is relatively independent of the Prandtl number at Rayleigh numbers greater than a finite critical value R_2 of the order of 5×10^3. At $R = 10{,}000$ the convective heat transport varies by only about 30% for Prandtl numbers in the range investigated. As the Rayleigh number is increased above the critical value R_2, the streamlines of the convection flow become circular, independent of the horizontal wavelength as long as the latter is larger than or about equal to twice the height of the layer.

1. Introduction

The problem of thermal convection of a Boussinesq fluid in a horizontal layer heated from below is characterized by two non-dimensional parameters, the Rayleigh number and the Prandtl number. Since the Rayleigh number R is defined in such a way that the onset of convection occurs at a value R_c independent of the Prandtl number P, the latter usually plays a secondary role in the study of convection. But the influence of the Prandtl number on nonlinear properties such as the heat transport is significant and not yet well understood. In particular, in the limit of low Prandtl number, large discrepancies exist between various theoretical predictions for the convective heat transport. This paper and its companion paper (Busse & Clever 1980) are addressed to this problem.

Although heat transport by convection in liquid metals is important in many engineering applications, most studies of low-Prandtl-number convection have been motivated by astrophysical applications. Since Prandtl numbers in stars may be as low as 10^{-8}, while laboratory experiments are limited by $P \gtrsim 10^{-2}$, there is a strong need for theoretical extrapolations to the limit $P \to 0$. The simplest theoretical results are based on a perturbation theory which is valid for slightly supercritical values of the Rayleigh number. The calculations of Schlüter, Lortz & Busse (1965) indicate that the convective heat transport decays proportional to P^2 at a given small value of $R - R_c$ with one exception: convection in the form of two-dimensional rolls with stress-free upper and lower boundaries exhibits a heat transport independent of P. Similar results have been obtained more recently by Gough, Spiegel & Toomre (1975)

0022-1120/81/4665-2560 $02.00

from numerical calculations of high-Rayleigh-number convection based on a mean-field approximation. It is physically unreasonable that the large discrepancy of the heat transport caused by a modification of the boundary condition should persist over an extended range of the Rayleigh numbers. Indeed, Jones, Moore & Weiss (1976) discovered in the related case of axisymmetric convection that the convective heat transport tends to become independent of P when the Rayleigh number exceeds a second critical value R_2 which is of the order $1{\cdot}5\ R_c$. The low-amplitude convection mode changes in the neighbourhood of R_2 into a mode characterized by the property that the Jacobian between vorticity and stream function approximately vanishes. The disappearance of the nonlinear term in the vorticity equation permits a strong rise of the amplitude of convection which, in turn, yields a high heat transport. The same effect was demonstrated analytically by Proctor (1977) in the case of convection in a horizontal cylindrical tube heated from below.

Both the axisymmetric convection cell with stress-free boundaries of Jones *et al.* (1976) and the horizontal cylinder of Proctor (1977) represent rather special cases of convection and the question remains whether the phenomenon of a second critical Rayleigh number R_2 for the onset of inertial convection represents a general feature of convection in low-Prandtl-number fluids. In this paper, numerical results for two-dimensional convection in a horizontal fluid layer with rigid boundaries will be presented indicating the transition to inertial convection in low-Prandtl-number fluids and the disappearance of the Prandtl-number dependence of the heat transport at moderately high Rayleigh numbers. In the companion paper (Busse & Clever 1980), a simple boundary-layer model is derived which yields explicit asymptotic expressions in the small Prandtl-number limit in reasonably close agreement with the numerical results.

2. Mathematical formulation of the problem

A complete mathematical description of the problem has been given in an earlier paper (Clever & Busse 1974) and only a brief outline will be given here. The reader is referred to this earlier work for a detailed description of the analysis.

The theoretical description of two-dimensional convection rolls is based on the Navier–Stokes equations and the heat equation in the Boussinesq approximation. Using the layer thickness d, d^2/κ and $\Delta T/R$ as scales for length, time and temperature, equations (1)–(3) of Clever & Busse (1974; hereafter referred to as CB) are obtained. ΔT is the temperature difference between the boundaries of the layer and κ is the thermal diffusivity. The physical properties enter the non-dimensional description of the problem in the form of the Rayleigh and Prandtl numbers, defined by

$$R = \gamma g \Delta T d^3/\nu\kappa, \quad P = \nu/\kappa,$$

where γ is the thermal expansion coefficient, g the acceleration of gravity, and ν is the kinematic viscosity. The fact that the Boussinesq approximation reduces the equation of continuity to $\nabla \cdot \mathbf{v} = 0$ allows us to eliminate the latter by introducing the general representation for a solenoidal vector field

$$\mathbf{v} = \boldsymbol{\delta}\phi + \boldsymbol{\epsilon}\psi \equiv \nabla \times (\nabla \times \mathbf{k}\phi) + \nabla \times \mathbf{k}\psi,$$

where $\mathbf{k}$ is the unit vector opposite to the direction of gravity. After introducing a

Cartesian system of co-ordinates, with the z co-ordinate in the $\mathbf{k}$ direction and operating on the equation of motion with $\boldsymbol{\delta}\cdot$, we obtain the following equations for ϕ and θ.

$$\partial_y(\nabla^4\phi - \theta) = (1/P)(\partial^2_{yz}\phi\partial^2_{yy}\nabla^2\phi - \partial^2_{yy}\phi\partial^2_{yz}\nabla^2\phi), \tag{2.1a}$$

$$\nabla^2\theta - R\partial^2_{yy}\phi = \partial^2_{yz}\phi\partial_y\theta - \partial^2_{yy}\phi\partial_z\theta. \tag{2.1b}$$

Since we are interested in steady two-dimensional solutions, we have neglected the x and t derivatives. As shown in CB, the function ψ does not enter the problem in this case. The boundary conditions are given by

$$\phi = \partial_z\phi = \theta = 0 \quad \text{at} \quad z = \pm\tfrac{1}{2}. \tag{2.2}$$

The Galerkin technique is used for the solution of equations (2.1), and ϕ and θ are expanded in terms of orthogonal functions.

$$\phi = \sum_{\lambda\nu} a_{\lambda\nu}\cos(\lambda\alpha_y)g_\nu(z), \tag{2.3a}$$

$$\theta = \sum_{\lambda\nu} b_{\lambda\nu}\sin(\lambda\alpha_y)f_\nu(z), \tag{2.3b}$$

where the functions g_ν, f_ν satisfy the boundary conditions (2.2). The functions

$$f_\nu(z) = \sin\nu\pi(z-\tfrac{1}{2}), \quad \nu = 1, 2, \ldots$$

are alternating even and odd in z, as are the functions $g_\nu(z)$, which satisfy four boundary conditions and are given in CB. Finally, we note that the symmetry of the equations allows us to restrict ourselves to the subset of solutions for which the coefficients with odd values of $\lambda + \nu$ vanish. Actual computations are carried out by neglecting all coefficients with

$$\lambda + \nu > N. \tag{2.4}$$

An acceptable solution is obtained when N is sufficiently large such that the coefficients change very little as N is replaced by $N+2$.

3. Results and discussion

3.1. *Numerical convergence*

The results of the calculations for two-dimensional convection rolls at low Prandtl number presented in CB are extended to a larger range of Rayleigh and Prandtl numbers. This extension has been carried out by means of a new computer code permitting a much larger value of the truncation parameter N to be used in the numerical calculations. Whereas previous computations were restricted to $N \leqslant 16$, computations with N increasing up to 30 have since then been accomplished. The number of unknown coefficients $a_{\lambda\nu}$ and $b_{\lambda\nu}$ has thus increased from 136 to 465 and the computational time per solution has increased by about a factor of 40. For $N = 30$, approximately 40 minutes of computational time on an IBM 3033 are required.

The major factor restricting the range of Rayleigh and Prandtl numbers that can be investigated is the computational expense for obtaining solutions at large values of the truncation parameter N. Owing to the increased complexity of the flow and the tendency towards boundary layer formation as the Rayleigh number increases and the Prandtl number decreases, large values of N are necessary to resolve the details of the flow with sufficient accuracy. In table 1, the convergence of the Nusselt number

		Truncation parameter, N									
R	$R-R_c$	12	14	16	18	20	22	24	26	28	30
1850	142	1·00344	1·00344	—	—	—	—	—	—	—	—
1900	192	1·00684	1·00685	1·00685	—	—	—	—	—	—	—
2000	292	1·01974	1·01951	1·01955	—	—	—	—	—	—	—
2200	492	1·08086	1·07230	1·07000	1·06959	—	—	—	—	—	—
2500	792	1·22155	1·19520	1·18141	1·17545	1·17335	—	—	—	—	—
3000	1292	1·42890	1·39361	1·36864	1·35296	1·34416	1·33978	—	—	—	—
4000	2292	—	—	—	1·62479	1·60760	1·59614	—	—	—	—
6000	4292	—	—	—	1·96248	1·93782	1·91895	1·90414	1·89397	—	—
8000	6292	—	—	—	—	—	2·12917	2·11006	2·09548	—	—
10000	8292	—	—	—	—	—	2·28978	2·26685	2·24881	2·23386	2·22264

TABLE 1. Convergence of the Nusselt number with increasing values of the truncation parameter, N, for $P = 0{\cdot}01$.

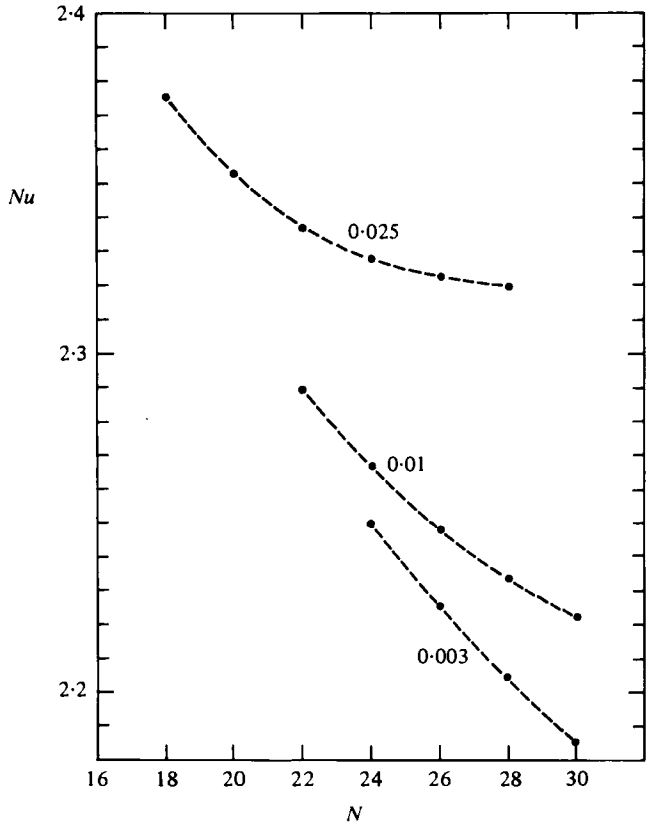

FIGURE 1. The convergence of the Nusselt number with increasing values of the truncation parameter, N, for various Prandtl numbers (given on curves) at $R = 10^4$ and $\alpha = \alpha_c$.

Nu with increasing values of N for various Rayleigh numbers is given in the case $P = 0{\cdot}01$. We note that although $N = 16$ is sufficient to converge the solution up to values of $R - R_c$ of the order of only several hundred, $N = 28$ or 30 is required for approximate convergence of the solution at Rayleigh numbers up to about 10^4. We note also that the convergence criterion used in CB, whereby the solution is considered to be converged when $Nu - 1$ changes by less than 2% as N is increased to $N + 2$, is insufficient for large values of N. A more appropriate criterion would be that $Nu - 1$ changes by less than 2% when N is increased by about 20%. According to this criterion, the solution for $P = 0{\cdot}025$ is well converged, as shown in figure 1, while the solution for $P = 0{\cdot}01$ is not far from its asymptotic value, as suggested by the significant second differentials of the computed values. On the other hand, the solution for $P = 0{\cdot}003$ is still quite far from a converged value. Because of the similarity of the curves in figure 1, an asymptotic value of the Nusselt number could be guessed by extrapolation. But this procedure has not been implemented.

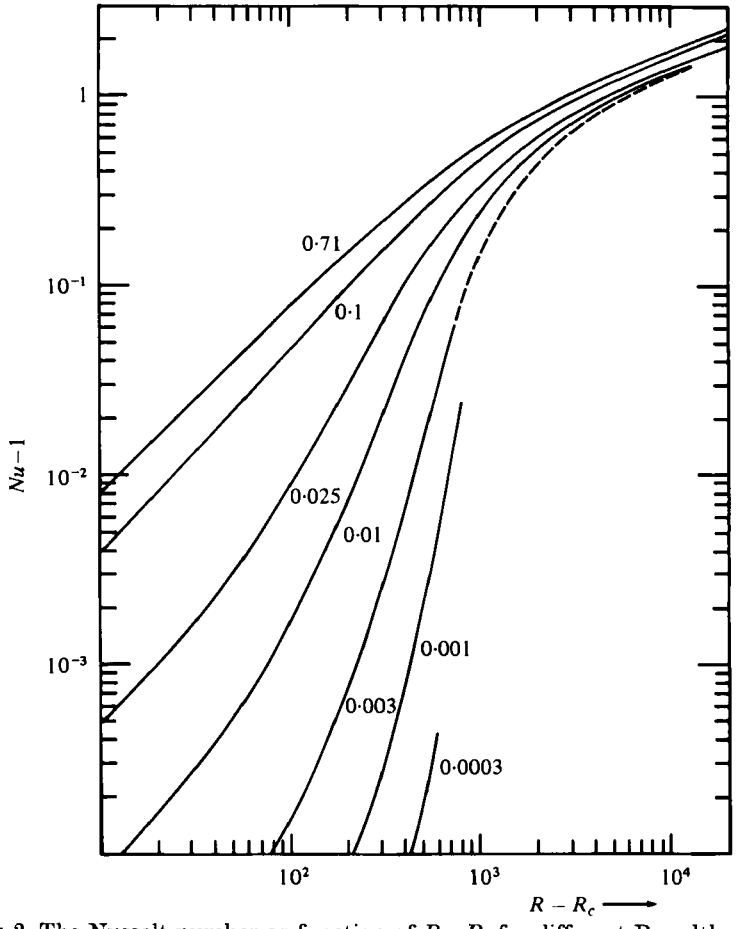

FIGURE 2. The Nusselt number as function of $R-R_c$ for different Prandtl numbers in the case $\alpha = \alpha_c$. Convergence of the solution for the dashed portion of the curve for $P = 0{\cdot}003$ is poorer than a few per cent.

3.2. *The heat transport*

Figure 2 exhibits the dependence of the Nusselt number on the Rayleigh number for Prandtl numbers in the range $3\times 10^{-4} \leqslant P \leqslant 0{\cdot}71$. The most striking feature is the contrast between the variation proportional to P^2 of $Nu-1$ at low values of $R-R_c$ and the near disappearance of any variation of Nu with P as R approaches 10^4. Three regions can be distinguished. The small amplitude region for which the perturbation results of Schlüter *et al.* (1965) are applicable is followed by a transition region as $R-R_c$ exceeds a value between 10 and 30. The rise of the heat transport in the transition region becomes steeper for decreasing Prandtl number in order that the large Prandtl-number value can be approached within a finite interval of the Rayleigh number. But it is difficult to say how large this interval is, since the curves shown in figure 2 approach each other relatively slowly as P decreases. Finally, at Rayleigh numbers approaching 10^4, the heat transport becomes nearly independent of the Prandtl number as shown in more detail in figure 3.

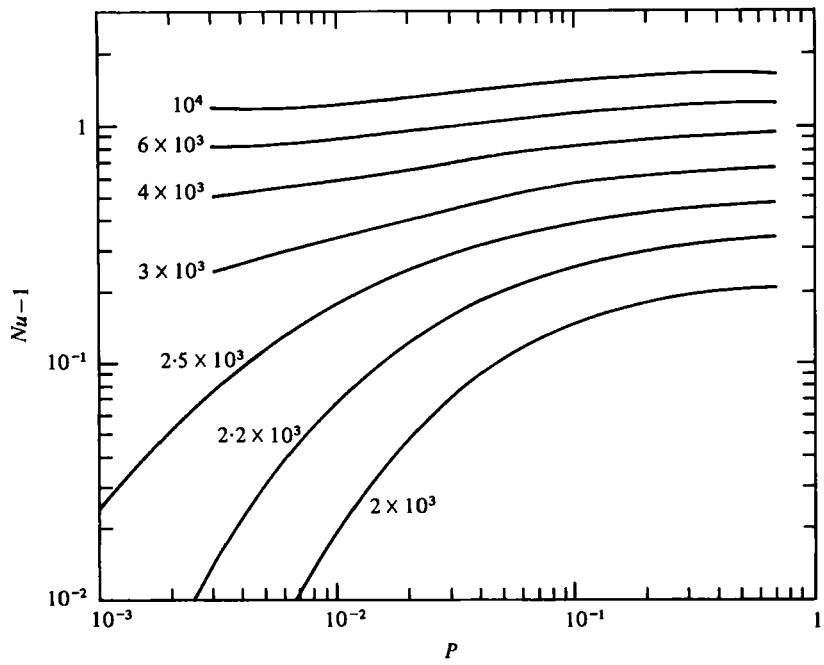

FIGURE 3. The dependence of the Nusselt number on the Prandtl number for selected values of R in the case $\alpha = \alpha_c$.

3.3. *The velocity field*

The origin of the sharp rise of the heat transport in the transition region is best understood in terms of the evolution of the streamline pattern of the velocity field as the Prandtl number decreases. Figure 4 demonstrates that the streamlines become more circular as P tends to zero. In the same limit, the lines of constant vorticity, $\omega \equiv \partial_y \nabla^2 \phi$, become approximately coincident with the streamlines, as shown in figure 5. To the extent to which ω is only a function of the stream function $\partial_y \phi$, the right-hand side of equation (2.1a) vanishes, since it can be written in the form

$$P^{-1}\{\partial_y \omega \partial_z \partial_y \phi - \partial_z \omega \partial^2_{yy} \phi\}. \tag{3.1}$$

Only the boundary conditions prevent the term (3.1) from vanishing entirely, and the high values that ω assumes in the boundary layers indicate that most of the viscous dissipation takes place there. Viscous and Reynolds stresses become of comparable order of magnitude near the top and bottom boundaries and balance the buoyancy force which is generated as the temperature diffuses from the boundaries into the interior and is advected by the flywheel-type motion.

The tendency towards a circular flow has been surprising in view of the highly anisotropic nature of the problem owing to the no-slip condition at top and bottom boundaries and the stress-free conditions on the side walls of the convection cells. In previous studies of 'flywheel' convection, as the circular motion has been called, the anisotropy was far less pronounced. In the problem of an axisymmetric convection cell in which the phenomenon of inertial convection was discovered by Jones *et al.* (1975), the anisotropy between the radial and vertical direction is relatively small

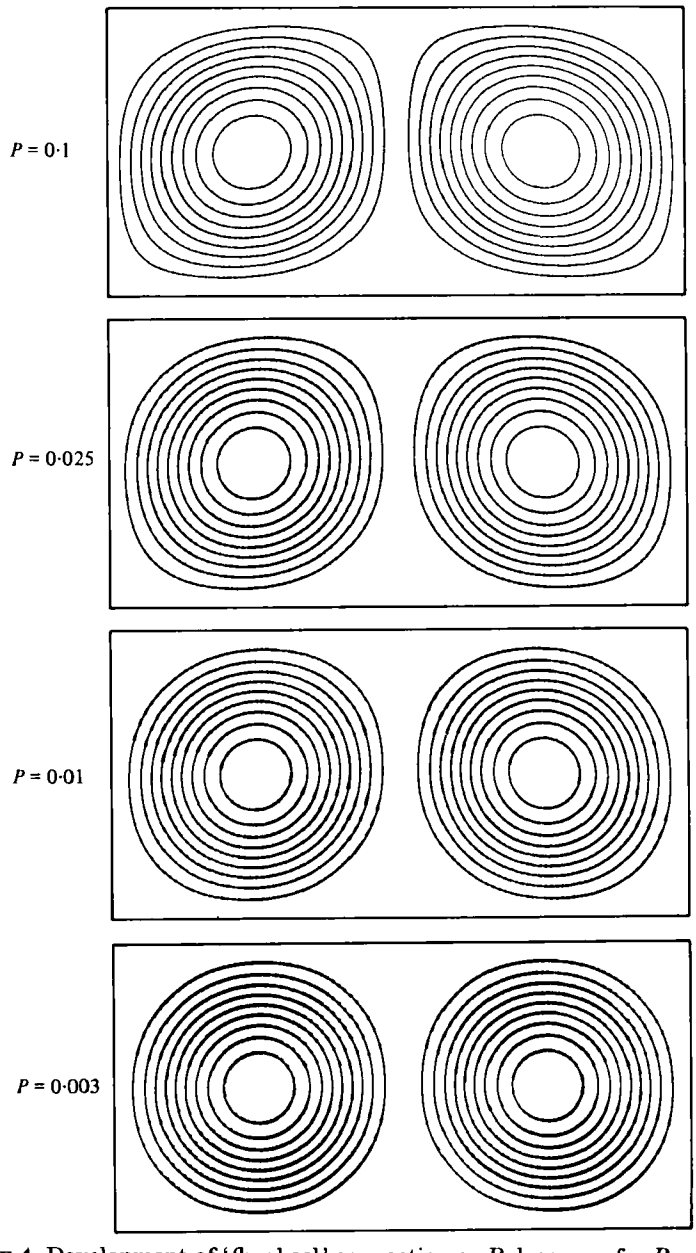

FIGURE 4. Development of 'flywheel' convection as P decreases for $R = 10^4$. The plots depict the stream function $\psi = \partial_y \phi$ at intervals of 1/10 of the maximum value. The flow of the right-hand roll is in the clockwise direction.

because stress-free conditions were imposed on all boundaries. A circular flow is most easily established in the example of a circular horizontal cylinder studied by Proctor (1977). Thus the impression prevailed that inertial or flywheel convection may only exist as a special phenomenon under favourable conditions. The present results challenge this impression and indicate the possible realization of 'flywheel'-convection rolls under general circumstances.

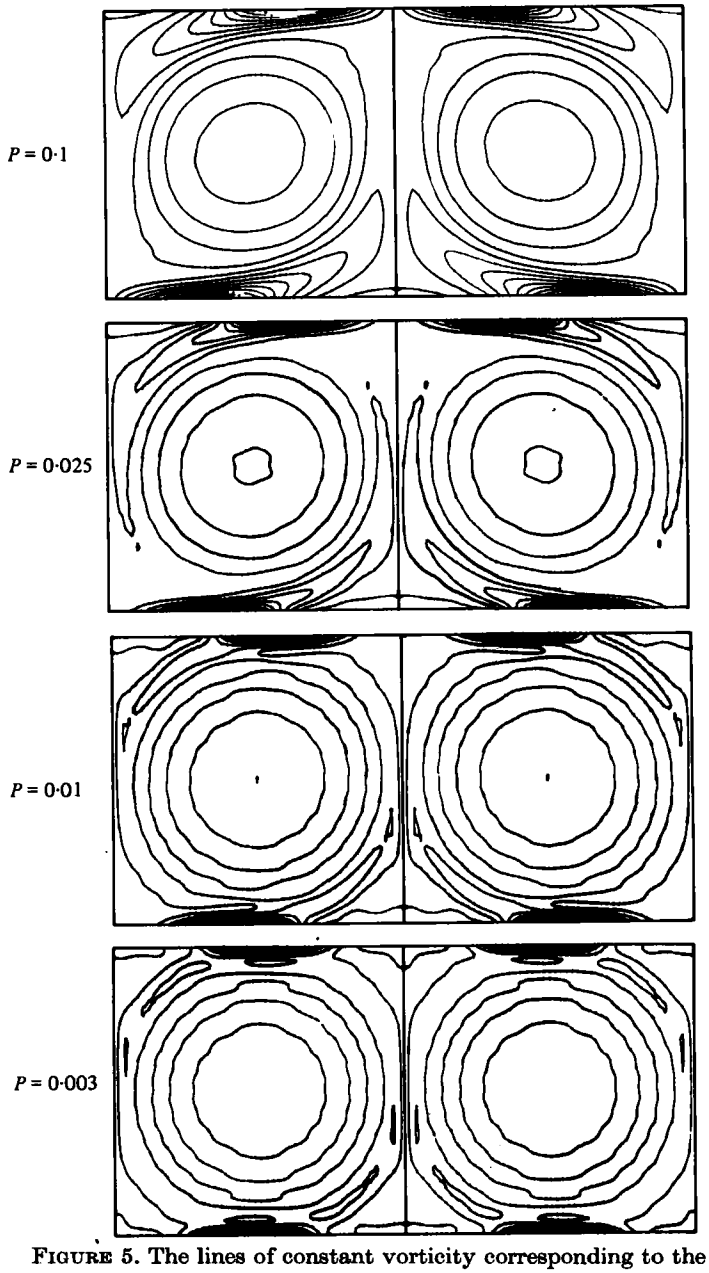

FIGURE 5. The lines of constant vorticity corresponding to the cases shown in figure 4.

The extent to which the motion becomes circular is shown in figure 6, where the x dependence of the z component and the z-dependence of the x component of the velocity field are compared. The different boundary conditions affect the profiles only in a small boundary-layer region. The isotherms shown in figure 7 do not seem to differ much from corresponding isotherms in high-Prandtl-number convection. The major effect of the decreasing Prandtl number seems to be the slight dip in the isotherms of

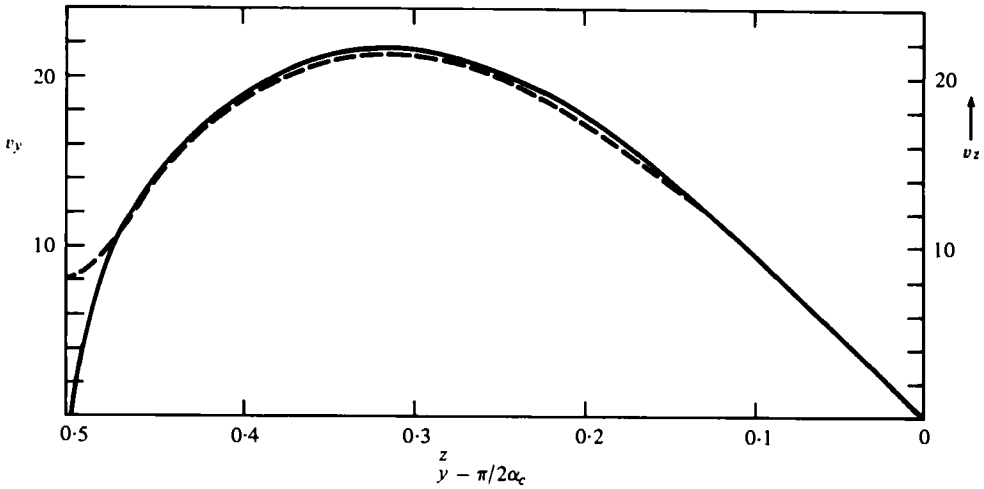

FIGURE 6. A comparison of v_y (solid) and v_z (dashed) for $0 \leqslant z \leqslant 0{\cdot}5$ and $-(\pi/6{\cdot}234) \leqslant y \leqslant 0$, at $y = 0$ and $z = 0$, respectively, in the case $R = 10^4$ and $P = 10^{-2}$.

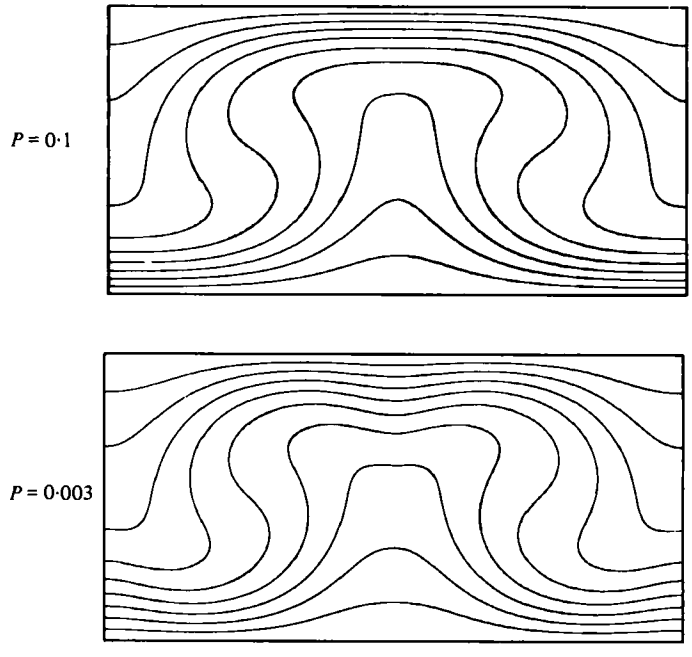

FIGURE 7. The isotherms of the temperature for $R = 10^4$, $\alpha = \alpha_c$ in the case $P = 0{\cdot}1$ and $P = 0{\cdot}003$.

the rising hot plume and of the descending cold plume which is caused by the relatively low value of the vertical velocity at the boundary of the roll. The circular flow is still realized when the horizontal wavelength $2\pi/\alpha$ exceeds the value of about 2, which is characteristic for the onset of convection. Figure 8 indicates that very little motion exists between the circular rolls and the temperature distribution does not deviate much from the static state in that region. The vanishing of expression (3.1) does not

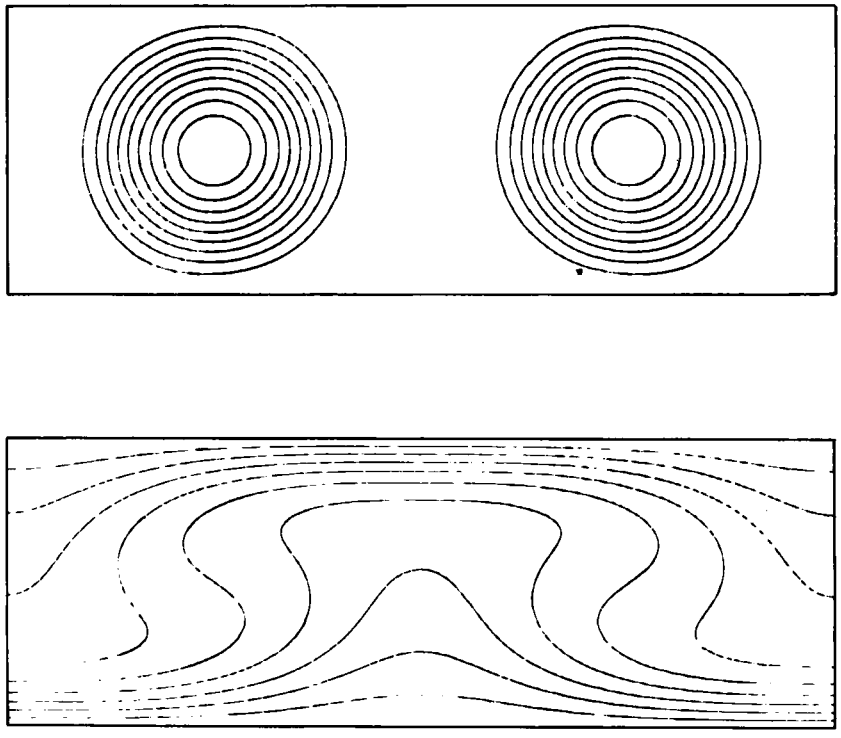

FIGURE 8. Streamlines ($\partial_y \phi$ = const.) and isotherms for $\alpha = 2{\cdot}2$, $P = 0{\cdot}025$, $R = 10^4$.

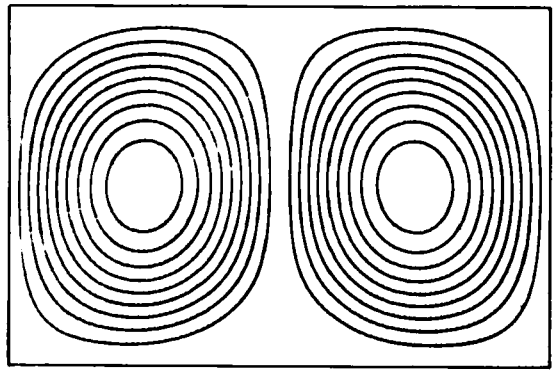

FIGURE 9. Streamlines ($\partial_y \phi$ = const.) at intervals of 1/10 of the maximum value for $R = 10^4$, $P = 0{\cdot}025$, $\alpha = 4{\cdot}2$.

require circular streamlines, although the latter seem to be preferred as the just-discussed example indicates. A circular flow would actually be rather inefficient in transporting heat if the diameter of the roll is less than the height of the layer which would be required for wavelengths $2\pi/\alpha$ less than 2. In this case, elliptically shaped streamlines occur as shown in figure 9. The fact that the corresponding heat transport is even larger than in the case of circular streamlines is surprising, but fits into the general trend that the maximum of the heat transport is always reached for wavenumbers

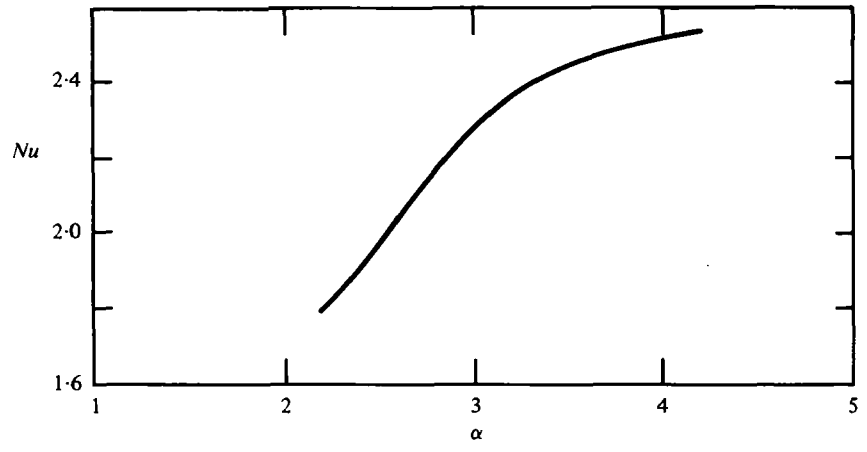

FIGURE 10. The dependence of the Nusselt number on the wavenumber α for $P = 0{\cdot}025$ and $R = 10^4$.

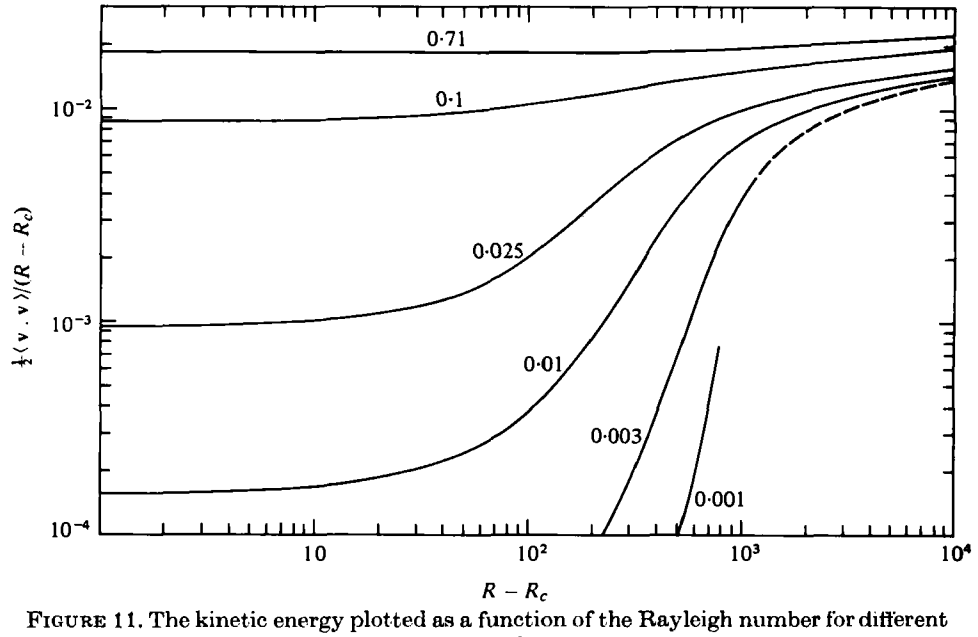

FIGURE 11. The kinetic energy plotted as a function of the Rayleigh number for different Prandtl numbers in the case $\alpha = \alpha_c$.

larger than α_c. A particular example of the dependence of the heat transport on the wavenumber α is shown in figure 10. The relatively sharp decay of the convective heat transport towards low wavenumber is essentially a geometrical effect. Since the 'flywheel'-convection rolls fill only the fraction α/π of the layer the convective heat transport is decreased by about the same fraction from the value at $\alpha \approx \pi$.

Besides the heat transport, the mean kinetic energy of motions is the most important integral property of convection. Since both properties are related to each other, it is not surprising that the dependence of $K \equiv \frac{1}{2}\langle \mathbf{v} \cdot \mathbf{v} \rangle$ on the Rayleigh number exhibits a similar variation with the Prandtl number as the heat transport. Figure 11 demonstrates that K varies proportional to P^2 for a low value of $R - R_c$, while it becomes

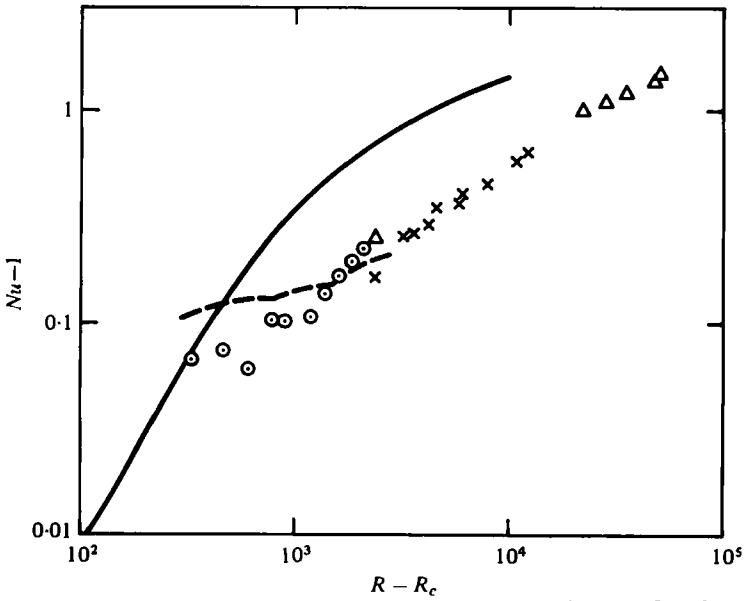

FIGURE 12. The dependence of the heat transport on the Rayleigh number for convection in mercury ($P = 0{\cdot}025$). The numerical results ($\alpha = \alpha_c$, solid curve) are seen in comparison with experimental measurements of Krishnamurti (1974), given by the dashed line, and of Rossby (1969) in which case data for layers of depth $d = 0{\cdot}19$ cm (⊙), $d = 1{\cdot}0$ cm (×), $d = 1{\cdot}8$ cm (△) are shown.

nearly independent of P as R approaches values of the order 10^4. The same figure also indicates that K increases nearly proportional to $R-R_c$ at high values of R.

4. Concluding remarks

The lowest Prandtl number for which experimental measurements of convective heat transport in a layer heated from below have been obtained is 0·025 corresponding to mercury. Experiments with liquid sodium could yield data for Prandtl numbers as low as 0·01, but this has not yet been achieved to our knowledge. It is difficult for several reasons to compare the experimental measurements with numerical results of the kind presented in this paper. Even in high-Prandtl-number fluids, additional information about the convection flow such as the wavelength of the convection rolls is needed before a sensible comparison can be made (Willis, Deardorff & Somerville 1972). In the case of mercury, the major difficulty is that convection rolls become unstable owing to the oscillatory instability at a Rayleigh number slightly above the critical value and certainly below the value for the onset of inertial convection. But there are indications that some kind of inertial convection is realized, even though the convection flow is time dependent and three dimensional. Rossby's (1969) data show clearly a very low convective heat transport at small values of $R-R_c$, while the slope of the Nu versus R curve is increasing for higher values of $R-R_c$ in distinct contrast to the results for high-Prandtl-number convection. Similar results have been obtained by Krishnamurti (1973). Although there seems some qualitative similarity between theory and experiment, a considerable discrepancy remains between the measured

data and numerical predictions as shown in figure 12. The numerical values have been obtained for $\alpha = \alpha_c$ and exceed the measured data by a factor of two for $R \gtrsim 3000$. But since this discrepancy is much smaller than if the prediction of the perturbation theory of Schlüter *et al.* would be used, it must be concluded that a mechanism similar to inertial convection takes place in the three-dimensional time-dependent convection flow realized in the experiment.

The research reported in this paper was supported by the Atmospheric Science Section of the U.S. National Science Foundation and by the Kernforschungszentrum Karlsruhe, West Germany.

REFERENCES

BUSSE, F. H. & CLEVER, R. M. 1980 An asymptotic model of two-dimensional convection in the limit of low Prandtl number. *J. Fluid Mech.* **102**, 75–83.

CLEVER, R. M. & BUSSE, F. H. 1974 Transition to time-dependent convection. *J. Fluid Mech.* **65**, 625–645.

GOUGH, D. D., SPIEGEL, E. A. & TOOMRE, J. 1975 Modal equations for cellular convection. *J. Fluid Mech.* **68**, 719.

JONES, C. A., MOORE, D. R. & WEISS, N. O. 1976 Axisymmetric convection in a cylinder. *J. Fluid Mech.* **73**, 353–388.

KRISHNAMURTI, R. 1973 Some further studies on the transition to turbulent convection. *J. Fluid Mech.* **60**, 285–303.

PROCTOR, M. R. E. 1977 Inertial convection at low Prandtl number. *J. Fluid Mech.* **82**, 97–114.

ROSSBY, H. T. 1969 A study of Bénard convection with and without rotation. *J. Fluid Mech.* **36**, 309–335.

SCHLÜTER, A., LORTZ, D. & BUSSE, F. 1965 On the stability of steady finite amplitude convection. *J. Fluid Mech.* **23**, 129–144.

WILLIS, G. E., DEARDORFF, J. W. & SOMERVILLE, R. C. J. 1972 Roll-diameter dependence in Rayleigh convection and its effect upon the heat flux. *J. Fluid Mech.* **54**, 351–367.